Science and Technology of Advanced Materials

ISSN: (Print) (Online) Journal homepage: www.tandfonline.com/journals/tsta20

Improvement in CPP-GMR read head sensor performance using [001]-oriented polycrystalline half-metallic Heusler alloy $Co_2FeGa_{0.5}Ge_{0.5}$ and CoFe bilayer electrode

Dolly Taparia, Taisuke Sasaki, Tomoya Nakatani, Hirofumi Suto, Yoshio Miura, Zehao Li, Varun Kumar Kushwaha, Kazuumi Inubushi, Shinto Ichikawa, Katsuyuki Nakada, Tomoyuki Sasaki, Seiji Mitani & Yuya Sakuraba

To cite this article: Dolly Taparia, Taisuke Sasaki, Tomoya Nakatani, Hirofumi Suto, Yoshio Miura, Zehao Li, Varun Kumar Kushwaha, Kazuumi Inubushi, Shinto Ichikawa, Katsuyuki Nakada, Tomoyuki Sasaki, Seiji Mitani & Yuya Sakuraba (2024) Improvement in CPP-GMR read head sensor performance using [001]-oriented polycrystalline half-metallic Heusler alloy $Co_2FeGa_{0.5}Ge_{0.5}$ and CoFe bilayer electrode, Science and Technology of Advanced Materials, 25:1, 2388503, DOI: 10.1080/14686996.2024.2388503

To link to this article: https://doi.org/10.1080/14686996.2024.2388503

Published online: 16 Aug 2024.

SCIENCE AND TECHNOLOGY OF ADVANCED MATERIALS
2024, VOL. 25, NO. 1, 2388503
https://doi.org/10.1080/14686996.2024.2388503

Improvement in CPP-GMR read head sensor performance using [001]-oriented polycrystalline half-metallic Heusler alloy $Co_2FeGa_{0.5}Ge_{0.5}$ and CoFe bilayer electrode

Dolly Taparia[a], Taisuke Sasaki[a], Tomoya Nakatani[a], Hirofumi Suto[a], Yoshio Miura[a], Zehao Li[a], Varun Kumar Kushwaha[a], Kazuumi Inubushi[b], Shinto Ichikawa[b], Katsuyuki Nakada[b], Tomoyuki Sasaki[b], Seiji Mitani[a] and Yuya Sakuraba[a]

[a]Research Center for Magnetic and Spintronic Materials, National Institute for Materials Science, Tsukuba, Japan;
[b]Advanced Products Development Center, Technology & Intellectual Property HQ, TDK Corporation, Ichikawa, Japan

ABSTRACT

A current-perpendicular-to-plane giant magnetoresistive (CPP-GMR) device with a half-metallic electrode is one of the most promising candidates of next-generation read head for hard disk drive. In this study, we fabricate [001]-oriented polycrystalline CPP-GMR devices with the normal ferromagnet (NFM) CoFe/half-metallic ferromagnet (HMFM) $Co_2FeGa_{0.5}Ge_{0.5}$ (CFGG) bilayer electrodes to enhance the magnetoresistance (MR) ratio by large interfacial spin-dependent scattering at the NFM/HMFM interface. The CoFe/CFGG bilayer electrode provides the additional large interfacial spin-dependent scattering and achieves high *MR* ratio of 22.7% with the CoFe(4.5 nm)/CFGG(2.5 nm) bilayer electrodes, which is almost three(two) times larger than the *MR* ratio with the single CoFe(CFGG) (7 nm) electrodes. The bias voltage dependent study revealed an additional advantage of increasing the output voltage $|\Delta V|$ by using the CoFe/CFGG bilayer due to the improvement of the endurance against spin-transfer torque under high bias current. A maximum output voltage $|\Delta V|_{max}$ of 6.5 mV was obtained with the CoFe(5.5 nm)/CFGG(1.5 nm) electrodes, which is the highest ever reported in the CPP-GMR devices with a uniform metallic spacer including high-quality epitaxial devices.

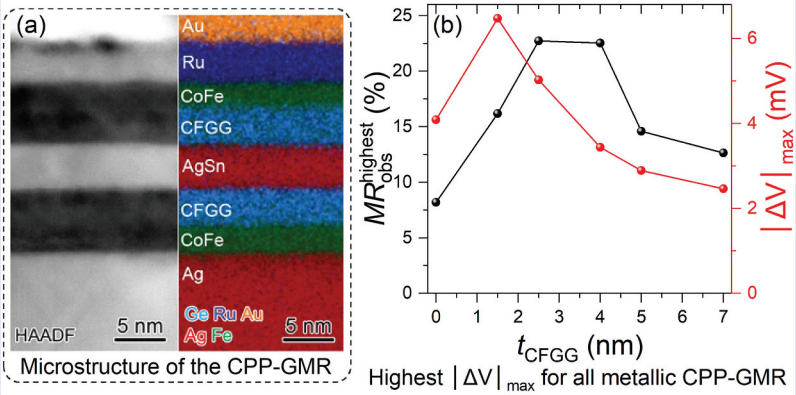

ARTICLE HISTORY
Received 20 May 2024
Revised 12 July 2024
Accepted 31 July 2024

KEYWORDS
Magnetic recording; read head; giant magnetoresistance; Heusler alloy; half-metal; spin-dependent scattering

IMPACT STATEMENT

Large improvement of MR ratio and the highest output voltage has been achieved in the polycrystalline CPP-GMR with the half-metallic $Co_2FeGa_{0.5}Ge_{0.5}$ and normal ferromagnetic CoFe bilayer electrodes.

1. Introduction

The ever-increasing surge of data demands for affordable and high capacity storage solutions. Hard disk drives, HDDs, are predicted to be the primary data repository for the foreseeable future [1]. Since the launch of the first hard disk drive (HDD) with a mere Mb-class storage capacity and an areal density of a few kb/in^2, HDDs has undergone a staggering increase in the areal density by an order of 10^8 and play an important role in today's digital landscape [2]. Modern technologies such as heat-assisted magnetic recording (HAMR) or bit-patterned media (BPM) are expected to further increase the areal density beyond 4

CONTACT Yuya Sakuraba SAKURABA.Yuya@nims.go.jp Research Center for Magnetic and Spintronic Materials, National Institute for Materials Science, Tsukuba 305-0047, Japan

Tb/in^2; thus, the development of next generation read heads with high magnetoresistance, *MR* ratio and low resistance-area product, $RA < 0.1\ \Omega\mu m^2$, are critical [1,3]. Present read head technology uses tunnel magnetoresistance (TMR) sensors due to their high *MR* ratio, but their high resistance caused by the tunneling barrier is a critical problem to further shrink the sensor size. CPP-GMR, which consists of an all-metallic multilayer structure with adjacent ferromagnetic (FM) and non-magnetic (NM) layers, is one of the most promising candidates because of its intrinsically low *RA*, allowing the read head to be designed for higher areal recording densities. In CPP-GMR, the dependence of change in *RA* between parallel and antiparallel configuration, (ΔRA), on bulk and interface asymmetry (β and γ) holds the key to develop a read head with high *MR* ratio [4]. It is essential to choose a magnetic material with high resistivity while still having a high spin-asymmetries [5]. The β is determined by the spin-polarization of the FM layer. As a result, half-metallic Co-based Heusler alloys with high spin-polarization are promising to improve the performance of CPP-GMR-based read heads [6,7]. In this regard, all-metallic [001]-oriented fully epitaxial Heusler alloy-based CPP-GMR devices have been widely investigated [8–12] For example, Li *et al.* reported a large *MR* ratio of 57% and ΔRA of 12 mΩ μm^2 in fully epitaxial $Co_2FeGa_{0.5}Ge_{0.5}$(CFGG)/Ag/CFGG-based CPP-GMR at room temperature (RT) [10]. Jung *et al.* further enhanced these results to 82% and 31 mΩ μm^2, respectively, by incorporating NiAl insertion layers [11]. Chikaso *et al.* also confirmed the enhancement of the *MR* ratio by using NiAl insertion layers in CFGG-based CPP-GMR devices [12]. However, the use of single crystalline MgO (001) substrate for these reported epitaxial devices and the necessity of high annealing temperature, T_a, greater than 500°C hinders the use for practical applications.

Another challenge is to achieve a high output voltage $|\Delta V|$ in a CPP-GMR device. At higher bias voltage (V_b), a CPP spin-valve is subject to the spin-transfer torque (STT) effect, which causes instability in the magnetization state of the free FM electrode. This decreases the *MR* ratio at higher V_b. Even with an *MR* ratio of 36% in the epitaxial $Co_2Fe_{0.4}Mn_{0.6}Si$ (CFMS)/$Ag_{83}Mg_{17}$/CFMS based CPP-GMR, the generated $|\Delta V|$ was of the order of 4.8 mV at $|V_b| = 38$ mV [13]. For all-metallic polycrystalline CPP-GMR of $Co_2Mn_{0.6}Fe_{0.4}Ge$(CMFG)/$Ag_{90}Sn_{10}$/CMFG [14] and CoFeGe(CFG)/$Ag_{84}Sn_{16}$/CFG [15], a small $|\Delta V|$ of 2.3 mV was achieved, which is due to the large STT effect and small magnetic damping constant in half-metallic Heusler electrodes [16,17]. A possible way to overcome this shortcoming of CPP-GMR sensors is the use of metal-oxide nanocomposite current-confined-path (CCP)-based spacer layer [14,18–22]. Nakatani *et al.* reported a high *MR* ratio of 54% and ΔRA of 75 mΩ μm^2 using polycrystalline CMFG as FM electrode and AgInZnO (AIZO) spacer precursor forming the Ag-In:Mn-Zn-O CCP spacer after annealing at $T_a = 280$°C. This method significantly increased $|\Delta V|$ to 18 mV due to the suppression of the STT by the CCP spacer [23]. Although high *MR* ratio and $|\Delta V|$ were achieved, the formation of non-uniform CCP along the metallic spacer layer causes a relatively large scattering of the device property in the same batch, which limits its integration in actual read head sensors. Therefore, we need to achieve high $|\Delta V|$ in the CPP-GMR with a uniform non-magnetic spacer.

Recently, Fujita *et al.* demonstrated a new approach to enhance *MR* ratio by large interfacial spin-dependent scattering at the normal ferromagnet (NFM)/half-metallic ferromagnet (HMFM) interface in the [001]-oriented fully epitaxial CPP-GMR with CoFe/CFMS bilayer FM electrodes and uniform Ag spacer [24]. They observed an increase of *MR* ratio from 28% with $Co_2Fe_{0.4}Mn_{0.6}Si$ (CFMS) single layer to 41% for CoFe/CFMS bilayer FM electrode. While this interfacial scattering is applicable to other half-metallic Heusler alloys and polycrystalline systems, such structures have not been explored. Additionally, the bilayer structure is expected to increase the $|\Delta V|$ by improving the tolerance to STT in the HMFM layer adjacent to an NFM with high magnetization and/or magnetic damping constant. Therefore, in this study, we fabricate all-metallic [001]-oriented polycrystalline CPP-GMR devices with CoFe/CFGG bilayer FM electrodes. CFGG was employed as the FM electrode instead of CFMS because of the higher *MR* ratio observed in epitaxial CFGG/Ag/CFGG-based CPP-GMR [10,24]. Also, a spacer of $Ag_{95}Sn_5$ was used due to the added advantages of higher corrosion endurance, lower roughness and longer spin-diffusion length as compared to the Ag spacer [25]. We investigate the effect of these CoFe/CFGG interfaces on the *MR* ratio and $|\Delta V|$, with the aim to realize practical polycrystalline CPP-GMR devices for read heads.

2. Methods

Pseudo spin-valves (PSV) with the stacking structure of Ta(5 nm)/Ag(100 nm)/CoFe(7-t_{CFGG} nm)/CFGG(t_{CFGG} nm)/$Ag_{95}Sn_5$(5 nm)/CFGG(t_{CFGG} nm)/CoFe(7-t_{CFGG} nm)/Ru(7 nm), with $t_{CFGG} = 0.0$, 1.5, 2.5, 4.0, 5.0 and 7.0 nm were deposited on thermally oxidized Si substrate at RT using an ultra-high vacuum compatible magnetron sputtering system with base pressure less than 1×10^{-7} Pa. To evaluate the effect of spin-dependent scattering at the CoFe/CFGG interface, the total film thickness was kept constant at 7.0 nm, while the ratio of the thickness of each CoFe and CFGG layer was varied. Substrate surface was cleaned

using reverse sputtering technique prior to deposition. The Ag buffer layer was deposited in $Ar + N_2$ atmosphere (10 and 25 sccm, respectively) to induce the growth along the [001]-direction [26]. The as-deposited films were *ex-situ* annealed at 300°C for 3 mins under high vacuum condition to reduce the interfacial roughness. The compositions of CFGG and CoFe layers were measured to be $Co_{47.6}Fe_{24.8}Ga_{15.0}Ge_{12.6}$ and $Co_{50}Fe_{50}$, respectively, by X-ray fluorescence spectroscopy (Rigaku Primus II). Electron beam lithography, photolithography and argon ion etching were used to pattern the films into circular and elliptical devices of varied pillar sizes ranging from 60×60 nm^2 to 200×100 nm^2. The pillars were defined using the electron beam lithography, whereas the bottom and top electrode fabrication was accomplished using photolithography. The actual pillar sizes were evaluated from the images of the pillars observed by scanning electron microscopy (SEM, Gemini). The crystal structure was determined *via* X-ray diffractometer (Rigaku, Smartlab) with Cu-K_α radiation ($\lambda = 1.5406$ Å). The microstructure of the CFGG layers and the interfacial flatness were analyzed using an aberration-corrected (scanning) transmission electron microscope ((S)TEM, FEI Titan G2 80–200). The magnetic property of the films was studied using vibrating sample magnetometer (VSM, Lake Shore Model 7410). The magnetoresistance (R – H) curve was measured at RT for each CPP-GMR device using dc four-probe method under a constant bias current *via* autoprober (TOEI) and manual prober.

3. Results and discussion

Based on our previous study on the growth of [001]-oriented polycrystalline CFGG thin film on Ag buffer layer deposited in $Ar + N_2$ atmosphere [26], we adopted the same approach for the present CPP-GMR films to realize a fully [001]-oriented stacking structure except for the Ru capping layer. Figure 1 shows the XRD pattern for various t_{CFGG}. The Ag buffer layer deposited in $Ar + N_2$ atmosphere successfully resulted in the preferred crystallographic orientation along the [001]-direction. The CFGG layer followed the buffer layer structure and a clear formation of the 002 superlattice peak at $2\theta = 31.33°$, representing the $B2$ phase was observed in CPP-GMR films for $t_{CFGG} = 4.0$, 5.0 and 7.0 nm. However, the 004 fundamental peak of CFGG and the 002 peak of CoFe overlaps with the 004 peak of thermally oxidized Si substrate, and as a result, the degree of $B2$ ordering could not be evaluated. Although no 002 peak for $t_{CFGG} = 2.5$ and 1.5 nm was seen, it does not exclude the presence of $B2$ ordered phase in the CFGG layer due to the limited detectability of the 002 peak in very thin CFGG layers by XRD.

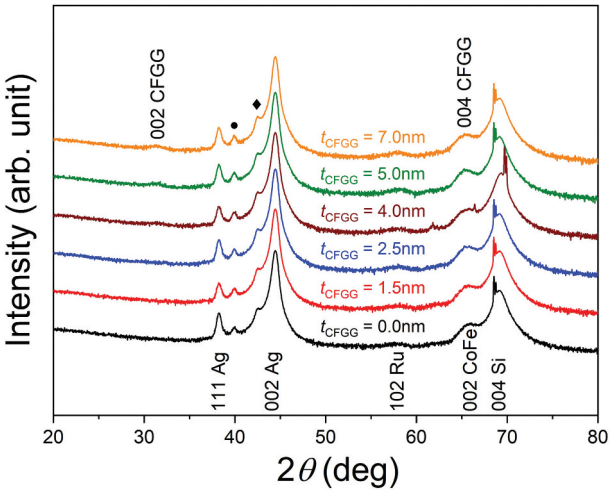

Figure 1. XRD pattern of 2θ-ω scan for the CPP-GMR films at various t_{CFGG}. The peaks represented by ♦ and • corresponds to the satellite peaks of 002 Ag generated by Cu-$K_{\alpha 1}$ and Cu-K_β X-ray wavelength.

The microstructure analysis was performed by TEM for the sample with $t_{CFGG} = 4.0$ nm. The high-angle annular dark-field (HAADF)-STEM image and Energy Dispersive Spectroscopy (EDS) elemental map in Figure 2(a,b) depicts flat interfaces, as Atomic Force Microscope (AFM) measurements confirmed smooth surfaces with average roughness, R_a, ≤0.5 nm for all films (not shown here). EDS elemental map clearly shows no significant intermixing of the CoFe and CFGG layers, and the line composition profile analyzed from Figure 2(c) shows that there is no significant interdiffusion of the constituent elements. Figure 2(d) shows the nanobeam diffraction patterns of the upper and lower CFGG and CoFe layers. Since the diffraction spots indicated by yellow triangle are visible in CFGG, they are identified as the (002) superlattice spots, indicating that CFGG layers have the $B2$-ordered structure, while the CoFe layer has the body-centered-cubic (*bcc*) structure. These nanobeam diffraction patterns also show that the [002] directions of the CoFe and CFGG layers are strongly aligned along the film normal direction.

MR curves of a total of 450 CPP-GMR pillar devices with different circular and ellipsoidal designed sizes were measured by the dc four-probe method with a constant bias current of +0.5 mA at RT. The direction of the positive bias current is defined as the direction in which the electrons flow from the bottom to the top FM electrode. The experimentally observed $\Delta R = R_{AP} - R_P$ are plotted in Figure 3(a–f) against R_P, where R_p and R_{AP} are the measured resistances in the parallel and antiparallel (AP) magnetization states, respectively. Figures 3(g–l) display the typical *MR* curves for each t_{CFGG}, where clear plateau region of the AP state is observed. The experimentally

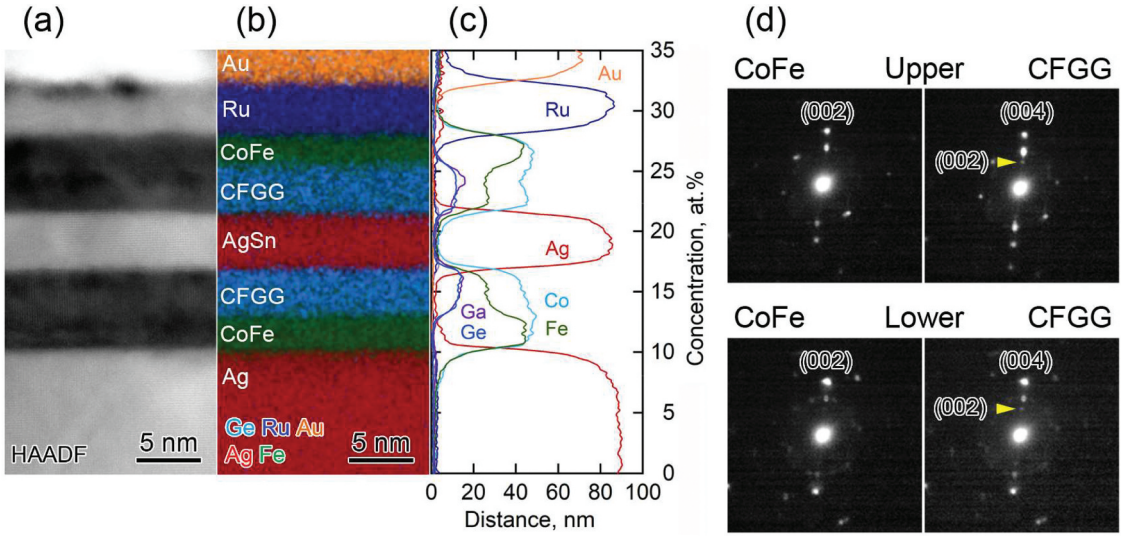

Figure 2. (a) Cross-sectional HAADF-STEM image and (b) corresponding EDS elemental map of Ag, Fe, Fe, Ru, and Au of the CPP-GMR stack. (c) Line compositional profile analyzed across the interfaces from EDS elemental map. (d) Nano beam diffraction patterns for upper CoFe and CFGG and lower CoFe and CFGG layers.

observed MR ratio (MR_{obs}) is defined as $\frac{\Delta R}{R_P}$. It is well known that the measured resistance of the CPP-GMR pillar always contains the intrinsic resistance of the pillar region (R_{pillar}) and the parasitic resistance (R_{para}) originating from electrode leads, thus $R_p = R_{pillar} + R_{para}$. Therefore, R_{para} reduces the MR_{obs} from the intrinsic MR ratio, $MR_{int}\left(=\frac{\Delta R}{R_{pillar}}=\frac{\Delta R}{R_P-R_{para}}\right)$, of the device. Thus, as indicated by the expression of $\Delta R = MR_{int}\left(R_P - R_{para}\right)$, the statistically averaged intrinsic MR ratio (MR_{int}^{avg}) and R_{para} can be estimated from the slope and x-intercept of the linear fitting of ΔR vs R_P plot, respectively. The data for all samples are well fitted by a linear function, and thus MR_{int}^{avg} and R_{para} were precisely evaluated for each t_{CFGG}. It should be mentioned that the range of R_p is different for each t_{CFGG} due to the different RA as shown in Figure 4(b).

Figure 4(a,b) shows the t_{CFGG} dependence of MR_{int}^{avg} and highest MR_{obs} ($MR_{obs}^{highest}$) and ΔRA and RA, respectively. In this study, the observation of the CPP-GMR pillars using scanning electron microscopy (SEM) revealed that the actual area of the pillars was greater than their designed size. Therefore, the observed area, A, was used to evaluate ΔRA and RA. Moreover, it was confirmed that the area of the pillars designed to have the same size varied, which resulted in the scattering of the ΔRA and A. This scattering has been incorporated in the error bar in Figure 3(b). For $t_{CFGG} = 0.0$ nm, MR ratio and ΔRA are determined by the spin-dependent scattering inside the CoFe electrode and at the CoFe/$Ag_{95}Sn_5$ interface; thus, the MR ratio and ΔRA are the lowest for these samples. Notably, as t_{CFGG} changed from 0.0 to 1.5 nm, $MR_{int}^{avg}\left(MR_{obs}^{highest}\right)$ and ΔRA exhibited a substantial increase from 6.4% (8.2%) and 1.6 $m\Omega \cdot \mu m^2$ to 14% (16.2%) and 3.4 $m\Omega \cdot \mu m^2$. With increasing the t_{CFGG} further to 2.5 nm, the $MR_{int}^{avg}\left(MR_{obs}^{highest}\right)$ increased to 17.1% (22.7%), which is maintained up to $t_{CFGG} = 4$ nm as 16.8% (22.5%). The ΔRA increased to 5.1 $m\Omega \cdot \mu m^2$ and 6.6 $m\Omega \cdot \mu m^2$ for $t_{CFGG} = 2.5$ nm and 4.0 nm, respectively. This MR ratio is comparable to the highest reported for any polycrystalline CPP-GMR with uniform NM spacer, annealed at $T_a \leq 300$°C [27]. When the $t_{CFGG} \geq 5.0$ nm, both $MR_{int}^{avg}\left(MR_{obs}^{highest}\right)$ and ΔRA rapidly decreased. Interestingly, the device with only half-metallic CFGG electrode ($t_{CFGG} = 7.0$ nm) shows smaller MR ratio and ΔRA than the sample with $t_{CFGG} = 2.5$ and 4.0 nm, although the highest bulk contribution on MR due to high spin-polarization of the CFGG can be expected in this device. This behavior of the t_{CFGG} dependence indicates that the formation of the CoFe/CFGG bilayer gives rise to the additional spin-dependent scattering at the CoFe/CFGG interfaces, leading to an increase in the MR and ΔRA, as observed in the [001]-oriented fully epitaxial CoFe/CFMS interface [24]. To obtain the contribution of the CoFe/CFGG interface scattering on MR, the spin-momentum of the injected conductive electron to CFGG from the counter CFGG layer through $Ag_{95}Sn_5$ spacer must be preserved to reach the CoFe/CFGG interface. Therefore, the t_{CFGG} for the highest MR and ΔRA is determined by the spin-diffusion length of CFGG, t_{SDL}. Because the reported t_{SDL} for CFGG is ~2–3 nm [28,29], the largest MR ratio and ΔRA were obtained at $t_{CFGG} = 2.5$ and 4.0 nm. The trend of the RA vs t_{CFGG}

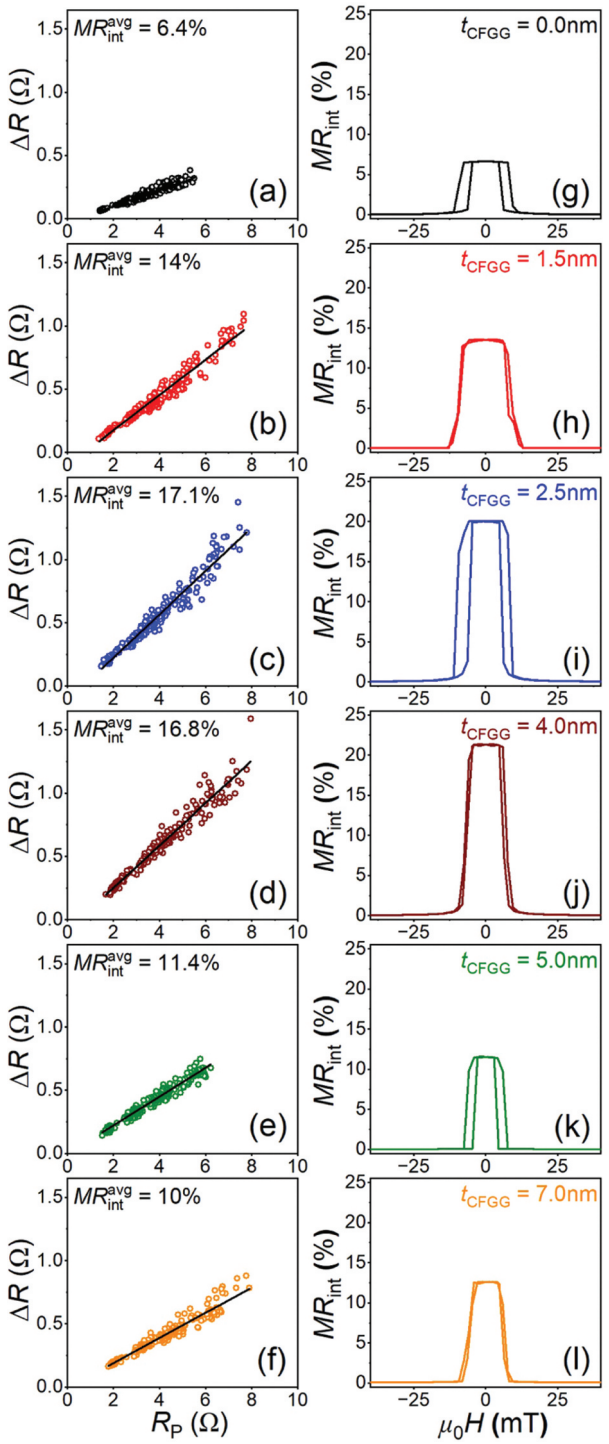

Figure 3. (a) – (f) Summary of the Δ*R* as a function R_p obtained by *R-H* curve measurement for all the devices for t_{CFGG} = 0.0, 1.5, 2.5, 4.0, 5.0 and 7.0 nm. The linear fitting curve to obtain MR_{int}^{avg} and R_{para} is also shown in each figure. (g) – (l) Typical MR_{int} curve after R_{para} subtraction for various t_{CFGG}.

is also qualitatively explained by the difference in the bulk resistivity between CoFe and CFGG, ρ_{CoFe} and ρ_{CFGG}. Namely, the sample with t_{CFGG} = 0.0 nm shows the smallest *RA* because of much smaller resistivity of CoFe than that of CFGG. The experimentally obtained ρ_{CoFe} and ρ_{CFGG} in the film annealed at 300°C are 18 and 139 $\mu\Omega \cdot cm$ respectively. This gives the difference of *RA* between t_{CFGG} = 0.0 and 7.0 nm originating from the resistance in FM layers as $(\rho_{CFGG} - \rho_{CoFe})t$ ~8.5 $m\Omega \cdot \mu m^2$, which is close to the experimentally observed difference, ~10 $m\Omega \cdot \mu m^2$. Because of large contribution of ρ_{CFGG} on total *RA*, the effect of the interface resistance at the CoFe/CFGG is not remarkable and almost monotonic increase of *RA* was observed. It is reasonable to consider that small peak appearing at t_{CFGG} = 4.0 nm is within the error in the monotonic increase of *RA* with t_{CFGG}.

For read head application, it is important to investigate the dependence of *MR* ratio on the applied V_b. Therefore, we measured the V_b dependence of *MR* ratio by selecting the device showing similar resistance value along with high *MR* ratio in each t_{CFGG}. In CPP-GMR devices, large V_b reduces *MR* due to the creation of an imperfect AP state induced by STT effect. Nakatani *et al.* reported that a bias direction to flow the electron from top to bottom FM layers is preferred to reduce the effect of STT and obtain high $|\Delta V|$ [14]. This is relevant to our CPP-GMR because of larger size of bottom FM electrode in tapered shaped pillar device. In our measurement, when the device is under negative biasing, the electrons flow from top to bottom electrode. Thus, negative bias voltage dependence of *R-H* curve was measured for the representative device in each sample with different t_{CFGG}.

From the *R-H* curves, MR_{obs} and *MR* normalized by the value at low V_b $(=[MR_{obs}/MR_{obs}^{max}])$ were calculated and plotted with respect to V_b in Figure 5(a,b) respectively. Both MR_{obs} and normalized *MR* decreased with increasing V_b. The two phenomena responsible for a decrease in the MR_{obs} are (i) Joule heating and (ii) STT-induced destabilization of the AP state. Joule heating, caused by increased power dissipation, elevates the device temperature, impacting its resistance and weakening the AP state. Additionally, higher negative bias in AP state gives larger STT to change the magnetization direction of bottom FM electrode and destabilize the AP state, and thus contribute to further lowering the *MR* ratio.

The *MR* ratio for t_{CFGG} = 0.0 nm remained stable even at a high V_b, reaching a maximum value, V_b^{max}, of −60 mV (Figure 5(b)). Here, V_b^{max} refers to the maximum V_b that can be applied before a 5% decrease in *MR* ratio is observed. The high V_b^{max} can be attributed to the higher saturation magnetization of the bottom CoFe electrode (Figure 5(c)) and the lower spin-polarization in the current generated from top CoFe electrode. At t_{CFGG} = 1.5 nm, V_b^{max} decreased to −35 mV. Addition of half-metallic CFGG layer led to a stronger spin-polarized current; also, the reduced saturation magnetization of the bottom CFGG/CoFe electrode decreased the tolerance against STT. Consequently, further increase in t_{CFGG} beyond 1.5 nm accelerated the decline in *MR* ratio due to the increasingly dominant STT effect.

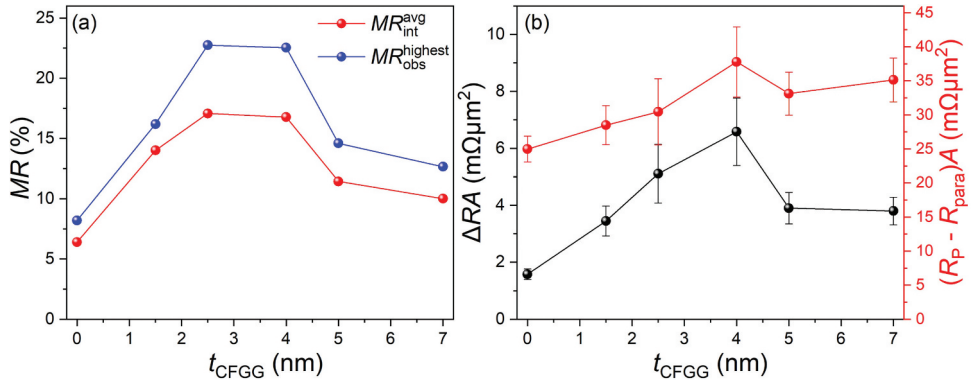

Figure 4. The t_{CFGG} dependence of (a) MR_{int}^{avg} and $MR_{obs}^{highest}$ and (b) Δ*RA* and *RA*.

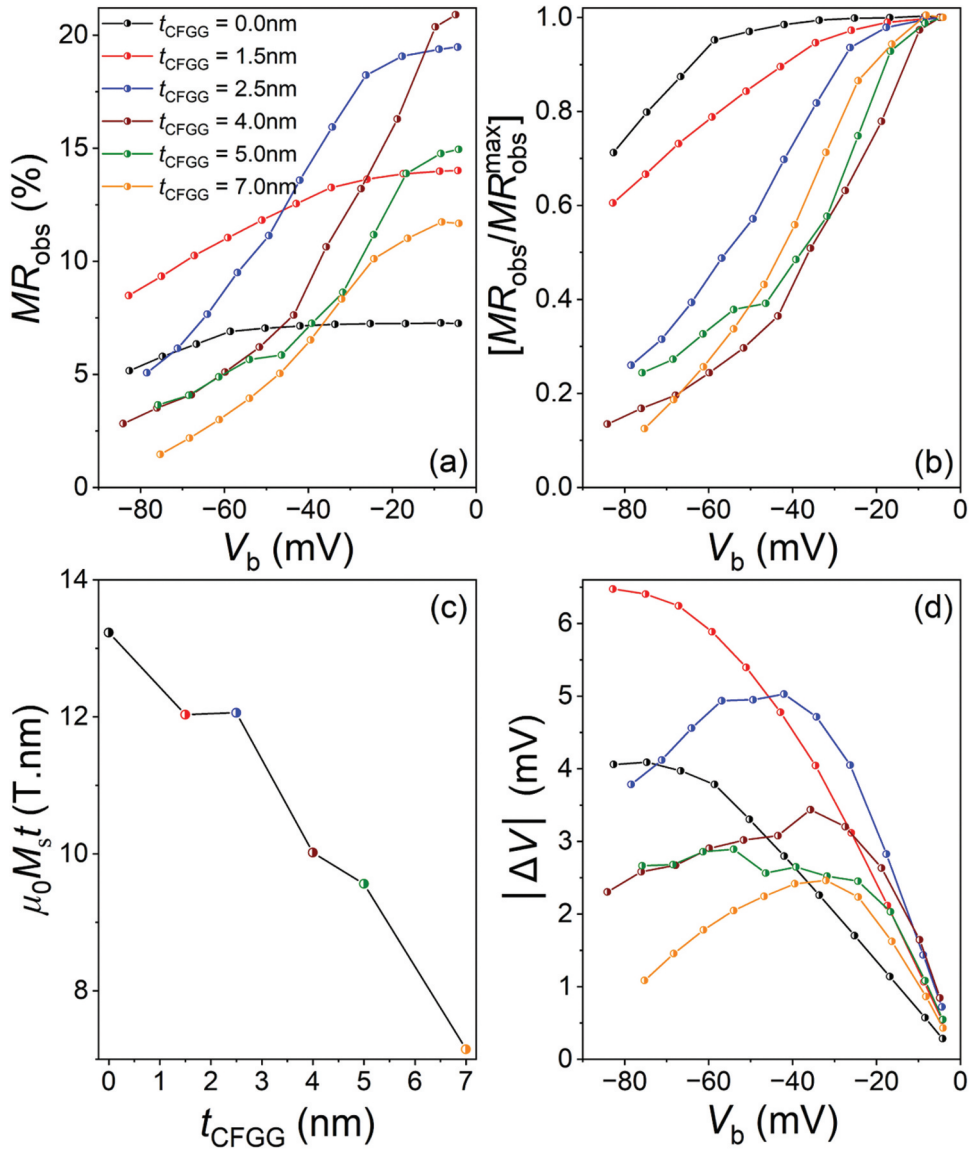

Figure 5. Variation of (a) MR_{obs}, (b) normalized *MR,* respectively, as a function of V_b for various t_{CFGG}, (c) saturation magnetization per area, $\mu_0 M_s t$, of CoFe/CFGG electrode as function of t_{CFGG}, and (d) output voltage, $|\Delta V|$, dependence on the biasing voltage, V_b, for various t_{CFGG}.

The read head output voltage, $|\Delta V| = MR_{obs} \times V_b$, was characterized as a function of V_b at different t_{CFGG} (Figure 5(d)). $|\Delta V|$ exhibits a distinct behavior: it initially increased linearly with V_b but then undergoes a sudden drop at a specific voltage threshold, V_b^t, beyond which the output voltage decreased for all devices regardless of t_{CFGG} thickness. It is important to note that, while $t_{CFGG} = 2.5$ and 4.0 nm gave

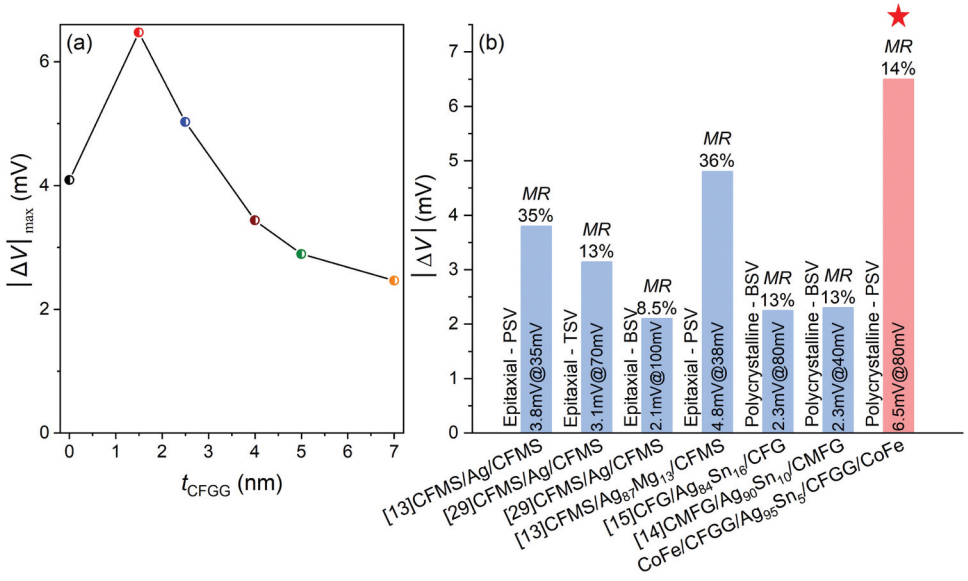

Figure 6. (a) Dependence of $|\Delta V|_{max}$ on t_{CFGG}, and (b) summary of $|\Delta V|_{max}$ reported for various all-metallic CPP-GMR devices. Here, PSV, TSV and BSV stands for pseudo spin-valve, top pinned spin-valve and bottom pinned spin-valve, respectively. The values inside the bars represent $|\Delta V|_{max}@|V_b^{max}|$.

a higher *MR* ratio, the highest $|\Delta V|$ was obtained for $t_{CFGG} = 1.5$ nm. This observation revealed the optimum thickness ratio of NFM and HMFM in the NFM/HMFM bilayer is different for obtaining the largest MR ratio at low V_b and the largest $|\Delta V|$. Thicker NFM having high magnetization (CoFe in present film) is suitable to make the device robust against STT, leading to higher $|\Delta V|$.

Figure 6(a,b) shows the variation of maximum output voltage, $|\Delta V|_{max}$, generated as a function of t_{CFGG} in present samples and the summary of $|\Delta V|_{max}$ reported in previous and current studies for all-metallic CPP-GMR devices with a uniform spacer, respectively. A $|\Delta V|_{max}$ of 6.5 mV was achieved at $V_b = -83$ mV for $t_{CFGG} = 1.5$ nm, the highest obtained value in the reported epitaxial and polycrystalline CPP-GMR devices with uniform spacer, which clearly indicates the strong advantage to obtain large $|\Delta V|$ in NFM/HMFM bilayer structure. It is important to note that bilayer NFM/HMFM electrode has two crucial roles to realize large $|\Delta V|$; one is the enhancement of *MR* ratio because of additional interface spin-dependent scattering and another is the improvement of the stability of magnetization against the STT induced by large V_b due to the high magnetization of NFM layer. In this study, the synergy of these two advantages enabled us to demonstrate the highest $|\Delta V|$ in the [001]-oriented polycrystalline CoFe/CFGG/$Ag_{95}Sn_5$/CFGG/CoFe PSV CPP-GMR device annealed at 300°C, which is grown on the practical Si substrate. This NFM/HMFM bilayer structure can be adapted to various stacking structures with different crystallographic directions and the conventional bottom-pin design of existing read heads, thus promising for realizing next-generation CPP-GMR-based read head technology.

4. Conclusion

We have investigated the role of spin-dependent scattering at NFM(CoFe, 7-t_{CFGG})/HMFM(CFGG, t_{CFGG}) interface in enhancing the *MR* ratio of [001]-oriented polycrystalline CPP-GMR device with uniform Ag spacer. The use of [001]-oriented Ag buffer layer enabled us to achieve strong [001] alignment throughout the CPP-GMR. *B*2-ordered phase in CFGG layers was confirmed by XRD and TEM. The CoFe/CFGG interface clearly worked to improve the *MR* values, reaching a maximum MR_{obs} of 22.7% for $t_{CFGG} = 2.5$ nm, which is comparable to the highest value ever reported in the polycrystalline CPP-GMR with a uniform NM spacer. Furthermore, the measurement of the bias voltage dependence of the *MR* property revealed that a high output voltage, $|\Delta V|$, of 6.5 mV under the bias voltage of −80 mV can be achieved in the device with $t_{CFGG} = 1.5$ nm due to the improvement of the stability of the AP magnetization state against the STT. Our results demonstrate that the optimization of the NFM/HMFM bilayer electrode can significantly improve the voltage output in practical polycrystalline CPP-GMR read heads.

Acknowledgments

The authors thank Dr. Y. Fujita and Dr. Z. Chen for their valuable insight and technical support. The authors also thank M. Maeda for her technical assistance in performing the Focused Ion Beam (FIB) lift-off for TEM observation.

Disclosure statement

No potential conflict of interest was reported by the author(s).

Funding

This work was supported by JSPS KAKENHI Grant No. [21H01608], MEXT Initiative to Establish Next-generation Novel Integrated Circuits Centers (X-NICS) Grant No. [JPJ011438], and JST CREST [Grant No. JPMJCR21O1].

References

[1] Albuquerque G, Hernandez S, Kief MT, et al. HDD reader technology roadmap to an areal density of 4 tbpsi and beyond. IEEE Trans Magn. 2022;58 (2):1–10. doi: 10.1109/TMAG.2021.3081042

[2] Piramanayagam SN, Chong TC, editors. Developments in data storage: materials prespective. John Wiley & Sons; 2011 Nov 8. https://www.wiley.com/en-us/Developments+in+Data+Storage%3A+Materials+Perspective-p-9780470501009

[3] Takagishi M, Yamada K, Iwasaki H, et al. Magnetoresistance ratio and resistance area design of CPP-MR film for 2–5 Tb/in^2 read sensors. IEEE Trans Magn. 2010;46(6):2086–2089. doi: 10.1109/TMAG.2010.2045739

[4] Valet T, Fert A. Theory of the perpendicular magnetoresistance in magnetic multilayers. Phys Rev B. 1993;48(10):7099–7113. doi: 10.1103/PhysRevB.48.7099

[5] Nagasaka K, Jogo A, Ibusuki T, et al. CPP-GMR technology for future high-density magnetic recording. Fujitsu Sci Tech J. 2006;42(1):149–157.

[6] Miura Y, Nagao K, Shirai M. Atomic disorder effects on half-metallicity of the full-heusler alloys $Co_2(Cr_{1-x}Fe_x)Al$: a first-principles study. Phys Rev B. 2004;69 (14):144413. doi: 10.1103/PhysRevB.69.144413

[7] Elphick K, Frost W, Samiepour M, et al. Heusler alloys for spintronic devices: review on recent development and future perspectives. Sci Technol Adv Mater. 2021;22(1):235–271. doi: 10.1080/14686996.2020.1812364

[8] Iwase T, Sakuraba Y, Bosu S, et al. Large interface spin-asymmetry and magnetoresistance in fully epitaxial Co_2MnSi/Ag/Co_2MnSi current-perpendicular-to-plane magnetoresistive devices. Appl Phys Exp. 2009;2(6):063003. doi: 10.1143/APEX.2.063003

[9] Sakuraba Y, Izumi K, Iwase T, et al. Mechanism of large magnetoresistance in Co_2MnSi/Ag/Co_2MnSi devices with current perpendicular to the plane. Phys Rev B. 2010;82(9):094444. doi: 10.1103/PhysRevB.82.094444

[10] Li S, Takahashi YK, Furubayashi T, et al. Enhancement of giant magnetoresistance by $L2_1$ ordering in $Co_2Fe(Ge_{0.5}Ga_{0.5})$ Heusler alloy current-perpendicular-to-plane pseudo spin valves. Appl Phys Lett. 2013;103(4):042405. doi: 10.1063/1.4816382

[11] Jung JW, Sakuraba Y, Sasaki TT, et al. Enhancement of magnetoresistance by inserting thin NiAl layers at the interfaces in $Co_2FeGa_{0.5}Ge_{0.5}$/Ag/$Co_2FeGa_{0.5}Ge_{0.5}$ current-perpendicular-to-plane pseudo spin valves. Appl Phys Lett. 2016;108(10):102408. doi: 10.1063/1.4943640

[12] Chikaso Y, Inoue M, Tanimoto T, et al. Effect of off-stoichiometric composition on half-metallic character of $Co_2Fe(Ga,Ge)$ investigated using saturation magnetization and giant magnetoresistance effect. J Phys D Appl Phys. 2022 Jun 9;55(34):345003. doi: 10.1088/1361-6463/ac73c1

[13] Narisawa H, Kubota T, Takanashi K. Current perpendicular to film plane type giant magnetoresistance effect using a Ag–mg spacer and $Co_2Fe_{0.4}Mn_{0.6}Si$ heusler alloy electrodes. Appl Phys Exp. 2015;8 (6):063008. doi: 10.7567/APEX.8.063008

[14] Nakatani T, Li S, Sakuraba Y, et al. Advanced CPP-GMR spin-valve sensors for narrow reader applications. IEEE Trans Magn. 2017;54(2):1–11. doi: 10.1109/TMAG.2017.2753221

[15] Mihajlović G, Read JC, Smith N, et al. Improved signal-to-noise ratio in current-perpendicular-to-plane giant magnetoresistance sensors using strong exchange-biased reference layers. IEEE Magn Lett. 2017;8:1–4. doi: 10.1109/LMAG.2016.2620119

[16] Oogane M, Kubota T, Naganuma H, et al. Magnetic damping constant in Co-based full heusler alloy epitaxial films. J Phys D: Appl Phys. 2015;48(16):164012. doi: 10.1088/0022-3727/48/16/164012

[17] Chumak OM, Pacewicz A, Lynnyk A, et al. Magnetoelastic interactions and magnetic damping in $Co_2Fe_{0.4}Mn_{0.6}Si$ and $Co_2FeGa_{0.5}Ge_{0.5}$ Heusler alloys thin films for spintronic applications. Sci Rep. 2021;11(1):7608. doi: 10.1038/s41598-021-87205-y

[18] Fukuzawa H, Yuasa H, Hashimoto S, et al. MR ratio enhancement by NOL current-confined-path structures in CPP spin valves. IEEE Trans On Magn. 2004;40(4):2236–2238. doi: 10.1109/TMAG.2004.829185

[19] Fukuzawa H, Yuasa H, Iwasaki H. CPP-GMR films with a current-confined-path nano-oxide layer (CCP-NOL). J Phys D: Appl Phys. 2007;40 (5):1213–1220. doi: 10.1088/0022-3727/40/5/S01

[20] Peng X, Kolbo P, Nikolaev K, et al. Current-confined-path (CCP) giant magnetoresistive (GMR) sensors. J Magn Magn Mater. 2009;321(12):1889–1892. doi: 10.1016/j.jmmm.2008.12.008

[21] Shimazawa K, Tsuchiya Y, Mizuno T, et al. CPP-GMR film with ZnO-based novel spacer for future high-density magnetic recording. IEEE Trans Magn. 2010;46(6):1487–1490. doi: 10.1109/TMAG.2010.2042574

[22] Nakatani T, Mihajlović G, Read JC, et al. High signal output in current-perpendicular-to-the-plane giant magnetoresistance sensors using In–zn–O-based spacer layers. Appl Phys Exp. 2015;8(9):093003. doi: 10.7567/APEX.8.093003

[23] Nakatani T, Sasaki TT, Sakuraba Y, et al. Improved current-perpendicular-to-plane giant magnetoresistance outputs by heterogeneous Ag-in: Mn-zn-O nanocomposite spacer layer prepared from Ag-in-zn-O precursor. J Appl Phys. 2019;126(17):173904. doi: 10.1063/1.5127176

[24] Fujita Y, Miura Y, Sasaki T, et al. Spin-scattering asymmetry at half-metallic-ferromagnet| ferromagnet interface. Phys Rev B. 2021;104(14):L140403. doi: 10.1103/PhysRevB.104.L140403

[25] Read JC, Nakatani TM, Smith N, et al. Current-perpendicular-to-the-plane giant magnetoresistance in spin-valves with AgSn alloy spacers. J Appl Phys. 2015;118(4):043907. doi: 10.1063/1.4927511

[26] Taparia D, Sasaki TT, Nakatani T, et al. Growth of polycrystalline Heusler alloy thin films using [001] textured Ag buffer layer for spintronics application. Available from: https://arxiv.org/abs/2405.08994

[27] Li S, Nakatani T, Masuda K, et al. Enhancement of current-perpendicular-to-plane giant magnetoresistive outputs by improving B2-order in polycrystalline $Co_2(Mn_{0.6}Fe_{0.4})Ge$ Heusler alloy films with the insertion of amorphous CoFeBTa underlayer. Acta Mater. 2018;142:49–57. doi: 10.1016/j.actamat.2017.09.046

[28] Goripati HS, Furubayashi T, Takahashi YK, et al. Current-perpendicular-to-plane giant magnetoresistance using $Co_2Fe(Ga_{1-x}Ge_x)$ Heusler alloy. J Appl Phys. 2013;113(4):043901. doi: 10.1063/1.4788672

[29] Diao Z, Chapline M, Zheng Y, et al. Half-metal CPP GMR sensor for magnetic recording. J Magn Magn Mater. 2014;356:73–81. doi: 10.1016/j.jmmm.2013.12.050